5-30-2014

Nd Isotopic Structure of the Pacific Ocean 70-30 and Numerical Evidence for Vigorous Ocean Circulation and Ocean Heat Transport in a Greenhouse World

Deborah J. Thomas
Texas A & M University - College Station

Robert Korty
Texas A & M University - College Station

Matthew Huber
Purdue University, mhuber@purdue.edu

Jessica A. Schubert
Texas A & M University - College Station

Brian Haines
Texas A & M University - College Station

AGU PUBLICATIONS

Paleoceanography

RESEARCH ARTICLE
10.1002/2013PA002535

Key Points:
- Results show deep water sinking in North and South Pacific during greenhouse
- Vigorous and separate overturning circulation in Atlantic and Pacific
- Strong vertical mixing may have enhanced ocean heat transport

Supporting Information:
- Readme
- Tables S1–S4

Correspondence to:
D. J. Thomas,
dthomas@ocean.tamu.edu

Citation:
Thomas, D. J., R. Korty, M. Huber, J. A. Schubert, and B. Haines (2014), Nd isotopic structure of the Pacific Ocean 70–30 Ma and numerical evidence for vigorous ocean circulation and ocean heat transport in a greenhouse world, *Paleoceanography*, *29*, 454–469, doi:10.1002/2013PA002535.

Received 15 JUL 2013
Accepted 28 APR 2014
Accepted article online 5 MAY 2014
Published online 30 MAY 2014

Nd isotopic structure of the Pacific Ocean 70–30 Ma and numerical evidence for vigorous ocean circulation and ocean heat transport in a greenhouse world

Deborah J. Thomas[1], Robert Korty[2], Matthew Huber[3], Jessica A. Schubert[1], and Brian Haines[2]

[1]Department of Oceanography, Texas A&M University, College Station, Texas, USA, [2]Department of Atmospheric Sciences, Texas A&M University, College Station, Texas, USA, [3]Department of Earth, Atmospheric, and Planetary Sciences, Purdue University, West Lafayette, Indiana, USA

Abstract The oceanic meridional overturning circulation (MOC) is a crucial component of the climate system, impacting heat and nutrient transport, and global carbon cycling. Past greenhouse climate intervals present a paradox because their weak equator-to-pole temperature gradients imply a weaker MOC, yet increased poleward oceanic heat transport appears to be required to maintain these weak gradients. To investigate the mode of MOC that operated during the early Cenozoic, we compare new Nd isotope data with Nd tracer-enabled numerical ocean circulation and coupled climate model simulations. Assimilation of new Nd isotope data from South Pacific Deep Sea Drilling Project and Ocean Drilling Program Sites 323, 463, 596, 865, and 869 with previously published data confirm the hypothesized MOC characterized by vigorous sinking in the South and North Pacific ~70 to 30 Ma. Compilation of all Pacific Nd isotope data indicates vigorous, distinct, and separate overturning circulations in each basin until ~40 Ma. Simulations consistently reproduce South Pacific and North Pacific deep convection over a broad range of conditions, but cases using strong deep ocean vertical mixing produced the best data-model match. Strong mixing, potentially resulting from enhanced abyssal tidal dissipation, greater interaction of wind-driven internal wave activity with submarine plateaus, or higher than modern values of the geothermal heat flux enable models to achieve enhanced MOC circulation rates with resulting Nd isotope distributions consistent with the proxy data. The consequent poleward heat transport may resolve the paradox of warmer worlds with reduced temperature gradients.

1. Introduction

The oceanic meridional overturning circulation (MOC) is responsible for a significant contribution of poleward heat transport in the modern climate system. Changes in the pattern and strength of the MOC are considered to have played a large role in past climate variations. However, the role of the MOC in greenhouse climate states presents a paradox. Classical theories [*Saenko*, 2006] predict that the MOC was weaker during greenhouse intervals that were characterized by reduced equator-to-pole temperature gradients [*Sluijs et al.*, 2006; *Zachos et al.*, 2008; *Hollis et al.*, 2009] since simple arguments suggest that MOC strength is proportional to density gradients [*Lyle*, 1997; *Huber and Sloan*, 2001; *Saenko*, 2006]. This implies a reduced contribution to the poleward oceanic heat transport during past greenhouse intervals, which is difficult to reconcile with overall polar warmth [e.g., *Sluijs et al.*, 2006; *Hollis et al.*, 2009].

Equally paradoxical is the role of MOC in global carbon cycling during warm intervals. Mechanisms proposed to explain periods of high organic carbon burial during the Late Cretaceous invoke either a sluggish [e.g., *Arthur et al.*, 1987] or a rapid MOC [e.g., *Martin et al.*, 2012]. However, organic carbon burial during the equally warm early Eocene was anomalously low [*Olivarez Lyle and Lyle*, 2006], perhaps implying a more rapid MOC [*Lyle*, 1997; *Hague et al.*, 2012]. Data that constrain the pattern and strength of the MOC are required to resolve these conflicting hypotheses.

Neodymium isotopes are one of the most robust tracers of ancient water mass composition, widely applied to timescales spanning the past ~400 Ma [e.g., *Frank*, 2002]. In this study, we pair new seawater and fine-grained detrital Nd isotope analyses with numerical simulations using general circulation models. Compilation of new Nd isotope data from South Pacific Deep Sea Drilling Project (DSDP) and Ocean Drilling Program (ODP) Sites 323, 463, 596, 865, and 869 with previously published data confirms strong convection in the South Pacific

as well as the North Pacific during the latest Cretaceous through early Paleogene (~70 to 30 Ma). Numerical simulations indicate deep water formation in both the South Pacific and North Pacific across a range of boundary conditions, though the strength and structure of the circulations vary with the imposed vertical-mixing profile.

2. Methods

2.1. Stratigraphic Recovery and Age Models for Drill Sites Investigated

DSDP Site 323 was cored in the central part of Bellingshausen abyssal plain in the eastern portion of the Pacific sector of the Southern Ocean (63°40.84′S, 97°59.69′W) at a water depth of 4993 m. The paleolatitude for Site 323 at ~ 63 Ma was 67°S, and the paleodepth evolved from ~2000 m during the Late Cretaceous and early Paleocene to nearly 4000 m (~35 Ma) [*Hollister et al.*, 1976]. The stratigraphic section investigated was recovered in Cores 14 through 18 (638.00–699.35 mbsf). The sediments recovered consist of red clays mostly barren of any microfossils [*Rogl*, 1976]. Accumulation rates for this sedimentary section were very low, ~15 m/Myr [*Hollister et al.*, 1976]. Shipboard investigation identified a hiatus spanning most of the Eocene in Cores 14 through 15 with the hiatus identified at 638.10 mbsf [*Hollister et al.*, 1976].

Biostratigraphically useful microfossils are rare throughout this section. Thus, we applied the closest biostratigraphic datums bounding the clay interval spanning our study section (Table S1 in the supporting information). Shipboard biostratigraphy assigned an age of 15 Ma to Core 7 core catcher sample (362.77 mbsf) based on the identification of the diatom *Denticula nicobarica* [*Hollister et al.*, 1976], and we apply this as the youngest age model tie point. In the absence of other age control, it might be reasonable to estimate ages based on typical accumulation rates for Pacific red clay sequences. However, a prominent hiatus punctuates the steady accumulation; therefore, we applied average accumulation rates for the intervals above and below the hiatus separately. The shipboard party assigned an age of 33.35 Ma to the sediment interval directly overlying the hiatus and assigned an age of 70 Ma to the sediment layer immediately overlying basement. We applied the shipboard estimated sedimentation rates of 15 m/Myr to the sequence above the hiatus and 5 m/Myr to the sequence between the hiatus and basement [*Hollister et al.*, 1976]. As it was not possible to convert the shipboard ages to the Geologic Time Scale (GTS 2004) [*Gradstein et al.*, 2005], we only treat these ages as broad estimates.

DSDP Site 463 was cored in the northwest Mid-Pacific Mountains (21°21.01′N; 174°40.07′E) in 2525 m of water. Its paleodepth was ~2000 m (~50 Ma) and paleolatitude was ~10°N. The investigated stratigraphic interval (41.41–47.84 mbsf) consists of foraminiferal and nannofossil chalk recovered in Cores 6 through 8. A ~17 Ma hiatus exists between the Oligocene and middle Eocene sections at ~41.00 to ~43.00 mbsf [*Thiede et al.*, 1981]. There is also a short hiatus in Core 7, section 3 (~46.80 mbsf) that encompasses most of the lower Eocene, and the entire Paleogene stratigraphic sections of the study interval [*Thiede et al.*, 1981].

Although sediments recovered at Site 463 contain abundant carbonate microfossils, little biostratigraphic information exists. Shipboard lithologic description and biostratigraphy identified a hiatus in Core 7 section 3 (46.8 mbsf) spanning the middle Eocene to Maastrichtian [*Thiede et al.*, 1981]. Shipboard nannofossil report for Paleogene ages above the unconformity [*Thiede et al.*, 1981]. The report only provides an estimate of the nannofossil zone of the recovered sections; therefore, we estimated the top and base of the respective zones from the shipboard report and applied the numeric ages of the NP zones from GTS 2004 [*Gradstein et al.*, 2005]. Below the unconformity we converted the Sr isotope values from *Barrera et al.* [1997] to GTS 2004 ages using the [*McArthur et al.*, 2001] Look-Up Table Version 4:08/04. All datums are detailed in the supporting information Table S1.

DSDP Site 596 is located in the southwest Pacific Ocean (23°51.20′S, 165°39.27′W) at a water depth of 5614 m. This site paleodepth was ~5000 m at 38°S in the South Pacific during the Paleocene (~54–62 Ma). The study interval was recovered in Cores 2 to 3 (12.0–23.83 mbsf) and consists of brown, zeolitic clay lacking biostratigraphically useful microfossils [*Winfrey et al.*, 1987]. We used constant Co accumulation age model [*Zhou and Kyte*, 1992] to assign numeric ages to the sediment intervals. The age model is tied to the Ir peak at the K/T boundary, so we updated the numeric ages to the GTS 2004 by adjusting the K/T age (Table S1 in the supporting information). This resulted in a constant offset of −0.9 Myr in the revised ages.

ODP Hole 865B was cored on Allison Guyot (18°26.41′N, 179°33.34′W), in the Mid-Pacific Mountains at a water depth of 1530 m. This site was located at or near the equator, ~5°N throughout the Paleocene and Eocene (~62–36 Ma) and at a paleodepth of 1500 m [*Sager et al.*, 1993]. The study interval spans the upper Paleocene to upper Eocene, between 18.15 and 134.32 mbsf and was recovered in Cores 3 through 15. The Paleogene sedimentary section consists of foraminiferal nannofossil ooze [*Sager et al.*, 1993], with nearly complete recovery of the Paleogene [*Bralower et al.*, 1995]. A detailed Paleogene nannofossil biostratigraphy exists for Hole 865B [*Bralower et al.*, 1995], and we converted the numeric ages to the GTS 2004 (Table S1 in the supporting information).

ODP Hole 869A was cored at Wodejebato Guyot in the equatorial Pacific Ocean (11°0.091′N, 164°44.969′E) at a water depth of 4826.7 m. Site 869 was situated at the equator at a paleodepth of 3600 m during the Eocene (~45 Ma) [*Sager et al.*, 1993]. The sampling interval for this investigation spans the upper Eocene to middle Eocene from 87.65 to 139.41 mbsf recovered from Cores 10 through 15. The primary lithology of the investigated sediments is clayey nannofossil and radiolarian ooze. Calcareous nannofossil biostratigraphy of Hole 869A indicates a hiatus in the upper middle Eocene and possibly also in the lower Oligocene [*Firth*, 1995]. We used the nannofossil datums [*Firth*, 1995] and applied the ages from the GTS 2004 for the Site 869 age model (Table S1 in the supporting information).

2.2. Nd Isotope Structure of the Modern Oceans

The Nd isotopic composition of seawater, expressed as ε_{Nd}, (the $^{143}Nd/^{144}Nd$ value of a geologic sample normalized to the bulk earth [*DePaolo and Wasserburg*, 1976]) varies on a basin scale as well as within individual ocean basins [*Piepgras and Wasserburg*, 1982, 1987; *Piepgras and Jacobsen*, 1988; *Jeandel*, 1993; *Jeandel et al.*, 1998; *Amakawa et al.*, 2000]. Surface seawater ε_{Nd} variations result from differences in weathering of subaerially exposed rocks that drain into a given ocean basin [*Goldstein et al.*, 1984; *Goldstein and Jacobsen*, 1987, 1988]. Intermediate and deep water masses acquire the isotopic composition of the surface waters in the region of subduction or downwelling [*Goldstein et al.*, 1984; *Goldstein and Jacobsen*, 1987, 1988; *Elderfield et al.*, 1990; *Halliday et al.*, 1992; *Sholkovitz*, 1993]. Subsequently, the initial ε_{Nd} of a particular water mass may be altered through mixing with other water masses or particle exchange processes [*Lacan and Jeandel*, 2001; *Siddall et al.*, 2008]; however, provenance information typically is retained because of the short oceanic residence time of Nd (~200–1000 years [e.g., *Tachikawa et al.*, 1999]) relative to overall oceanic mixing rates. Nonetheless, it is important to consider the effects of boundary exchange [e.g., *Lacan and Jeandel*, 2005; *Arzouse et al.*, 2007] and other contributions of dissolved Nd to seawater at depth when interpreting paleo-Nd isotope records in terms of water mass composition and overturning circulation patterns.

Modern North Atlantic Deep Water (NADW) has a ε_{Nd} signature of ~ −12 to −13, imparted by mixing of waters from the Nordic Seas (ε_{Nd} ~ −9) and the Labrador Sea with a surface ε_{Nd} value as low as ~ −26 [*Piepgras and Wasserburg*, 1987]. Modern Southern Ocean waters (both Antarctic Intermediate Water and Antarctic Bottom Water) have a more radiogenic signature of ~ −8 to −9, derived from the mixing of NADW with Pacific waters flowing eastward through the Drake Passage within the Circumpolar Current [*Piepgras and Wasserburg*, 1982]. Surface waters of the modern North and South Pacific have the most radiogenic ε_{Nd} values of ~0 to −4 [*Piepgras and Jacobsen*, 1988], and this reflects the average fluvial input to the Pacific of −2.9 to −3.7 [*Goldstein et al.*, 1984; *Goldstein and Jacobsen*, 1987, 1988].

Depth profiles of Nd isotopic composition indicate considerable stratification of South Pacific waters compared to the North Pacific. Analyses from the South Pacific indicate very radiogenic surface waters of ε_{Nd} ~0 underlain by lower ε_{Nd} values of ~ −8 at 4500 m water depth [*Piepgras and Jacobsen*, 1988]. The more negative bottom water signature reflects the northward flow of Antarctic bottom waters into the Pacific [*Piepgras and Wasserburg*, 1982; *Amakawa et al.*, 2009; *Tazoe et al.*, 2011; *Carter et al.*, 2012; *Stichel et al.*, 2012]. Much less stratification of ε_{Nd} values is evident in North Pacific profiles despite the existence of distinct intermediate, deep, and bottom water masses [*Talley*, 1993; *Tomczak and Godfrey*, 1994]. Overall slow deep water renewal in the North Pacific enables vertical exchange of Nd from Pacific surface waters to overprint the northward advecting Circumpolar Deep Water signal [*Piepgras and Wasserburg*, 1982], resulting in relatively radiogenic deep waters in spite of the absence of large-scale convection in the North Pacific.

2.3. Analytical Methods

The Nd isotopic composition of the water mass bathing a particular location is recorded and preserved by the teeth and bones of fossil fish [*Wright et al.*, 1984; *Shaw and Wasserburg*, 1985; *Staudigel et al.*, 1985; *Reynard et al.*, 1999; *Martin and Haley*, 2000; *Martin and Scher*, 2004; *Thomas*, 2005; *Thomas and Via*, 2007] as well as the disseminated authigenic oxide minerals [*Martin et al.*, 2010]. We analyzed both fish debris and leached oxide minerals in this study. To isolate fish debris, we disaggregated bulk sediment samples in a dilute solution of sodium metaphospate solution and washed through a >63 μm sieve. Then we handpicked teeth and fragments of fish debris, using ~20–30 fragments per sample depending on availability and size. Replicate samples were also picked from several sites. A significant body of work indicates that the rigorous reductive/oxidative cleaning protocol is not necessary, as oxide coatings record the same Nd isotopic signal as the biogenic apatite [*Martin et al.*, 2010; *Roberts et al.*, 2010; *Hague et al.*, 2012]. Therefore, prior to dissolution, we rinsed the samples twice in ethanol followed by two rinses in ultrapure water (Milli-Q).

To extract the disseminated oxide minerals, we decarbonated bulk, homogenized samples using 50 mL of 2.7% acetic acid buffered with Na acetate (pH 5) for 2 h on a shaker table. After carbonate digestion, samples were centrifuged and the supernatant discarded. The leaching procedure was repeated until all carbonate was digested. Following complete digestion, we rinsed samples 3 times in Milli-Q water. To leach the oxide fraction, we added 14 mL of buffered and chelated 0.02M Hydroxylamine Hydrochloride (HH) solutions and allowed the samples to react for 1.5 h on a shaker table. After centrifuging, the supernatant was retained and 40 mL of fresh HH solution was added to the samples for a long (24 h) extraction. Following the long extraction, samples were centrifuged; the supernatant was discarded and rinsed 3 times in Milli-Q water. The residual samples were dried and powdered for detrital silicate analysis of targeted samples.

Fish debris samples were dissolved in 2N HNO_3 for RE Spec chemistry. We dissolved the leachate samples in several milliliters of concentrated HNO_3 and dried down, then dissolved the samples in 2N HNO_3. Detrital silicate dissolution required the lengthy HF/HNO_3 dissolution followed by an HCl dissolution step. After drying down, we dissolved the detrital samples in several milliliters of concentrated HNO_3 and dried down, then dissolved the samples in 2N HNO_3. The rare earth elements from all fractions were isolated using RE Spec cation exchange column chemistry followed by Nd isolation from the bulk rare earth elements via methyllactic acid column chemistry.

All samples were loaded using 1 μL of 2N HCl onto a rhenium (Re) filament and analyzed on the Thermo Triton thermal ionization mass spectrometer as Nd^+. External precision was 15 ppm (2σ) with a value 0.512104 based upon replicate analysis of JNd_i standard ($n = 40$) over the course of this study. Using the numerical ages determined with the age models detailed above, $\varepsilon_{Nd}(t)$ values were calculated. For fish debris, we applied a typical $^{147}Sm/^{144}Nd$ value of 0.131 [e.g., *Thomas*, 2004]. We adopted the $^{147}Sm/^{144}Nd$ value of 0.109 for determination of the silicate $\varepsilon_{Nd}(t)$ values based on upper crustal average concentrations of Sm and Nd [*Taylor and McLennan*, 1995] and a $^{147}Sm/^{144}Nd$ value of 0.115 for the oxide fraction based on values reported for Fe-Mn crusts [*Ling et al.*, 1997].

2.4. MITgcm Simulations and Boundary Conditions

To run the MIT general circulation model (MITgcm) as an ocean model [*Marshall et al.*, 1997], boundary conditions for the surface were taken from two sets of previously coupled experiments [*Lunt et al.*, 2012] computed with the National Center for Atmospheric Research (NCAR) Community Climate System Model version 3 (CCSM3). Those experiments were forced with carbon dioxide (CO_2) levels of 2240 ppmv (hereafter "warm") and 4480 ppmv (hereafter "very warm"), which produced temperature profiles that compared favorably to proxy reconstructions from the middle and late Eocene and Paleocene and from the warmer early Eocene, respectively. As noted previously [*Huber and Caballero*, 2011], using radiative forcing this strong does not imply that CO_2 during the Paleogene must have been this high; rather, these are the levels necessary to achieve warmth consistent with proxy levels in a model whose climate sensitivity to doubling CO_2 is low. In both experiments, the solar constant was set to 1365 W/m^2, aerosol radiative effects were set to zero, and orbital parameters and other trace gas concentrations from preindustrial era conditions were used [*Liu et al.*, 2009]. Thus, the variations in CO_2 are solely responsible for the radiative changes leading to increasing surface temperatures, and they yield mean annual sea surface temperatures exceeding 35°C in the warmest equatorial regions, while high-latitude temperatures are ~10°C. The pattern of freshwater forcing shows

excess freshwater input from precipitation in tropical convection and middle-latitude storm tracks; in the subtropics, evaporation dominates.

We used seasonally varying climatologies of the surface temperature, wind, and salinity fields from both the 2240 ppmv (warm) and 4480 ppmv (very warm) simulations to force our own ocean simulations in the MITgcm. We used Paleogene continental configuration with 4° by 4° horizontal resolution and 18 vertical levels; the Gent-McWilliams and K-profile parameterizations were used. The simulations restore boundary conditions to the monthly varying temperature and salinity fields using a 30 day relaxation timescale; this tethers the surface conditions to those from the coupled model.

We used the passive tracer code within the MITgcm to estimate the Nd distribution implied for each case. Values are restored at the surface to a prescribed value, and then interior points are determined following advection and mixing by the interior flow. We restore values to −6 epsilon units in the South Pacific, +5 in the North Pacific, and −10 everywhere else. Data constraining the absolute surface water values do not exist; thus, these values are estimated based on existing deep water and detrital $\varepsilon_{Nd}(t)$. The −10 value is based on the range of early Paleogene $\varepsilon_{Nd}(t)$ values recorded by fine-grained detrital (eolian) inputs (~ − 8 to −12) to the tropical and subtropical Pacific [*Woodard and Thomas*, 2009; this study]. We apply −6 as the end-member value for the South Pacific based on the range of seawater values recorded at Sites 596 and Site 323 (~ − 5.0 to −5.6) once the seafloor had deepened between ~62 and 57 Ma (this study; please refer to section 3 for the details of this interpretation). This is a reasonable estimate given the southerly location of Site 323, as well as the values recorded at Site 596 to the north, reflecting mixing of Antarctic Peninsula weathering inputs with other source(s) of more unradiogenic surface water Nd in the Ross Sea region. The North Pacific end-member was estimated from the composition of radiogenic detrital $\varepsilon_{Nd}(t)$ values recorded at North Pacific Sites 192 and 883 [*Hague et al.*, 2012].

2.5. Construction of the Global Compilation Ocean "Section"

The proxy data were placed on to a regular latitude-depth grid based on their reconstructed depths and paleolocations (Table S2 in the supporting information) and the natural regridding routines from the NCAR Command Language were used to create interpolated, gridded values. Extrapolation beyond the convex hull of the kernel was not used. The ocean model Nd fields were resampled at the same paleodepths and paleolocations to enable a point-wise model-data comparison.

2.6. Reconstruction of the Meridional Temperature Gradient From Published Proxy Data

We compared model-generated meridional temperature gradients to a proxy compilation modified from *Hollis et al.* [2009] based on updated calibrations and refined estimates of seawater Mg/Ca values (Table S3 in the supporting information). The proxy data span a target age of 49–55 Ma (excluding the Paleocene-Eocene Thermal Maximum) to capture the very warm interval of the early Eocene.

3. Results and Discussion

3.1. Nd Isotope Data

The dissolved Nd isotopic composition recorded at Site 323 decreased from −3.6 at ~70 Ma to −5.3 by ~62 Ma (Figure 1 and Table S4 in the supporting information). This overall decrease coincides with the gradual deepening of the seafloor from ~2000 m to ~3000 m by ~62 Ma [*Hollister et al.*, 1976]. After ~62 Ma, the average seawater $\varepsilon_{Nd}(t)$ value at Site 323 was −5.4, similar to the range of values recorded by Site 596 to the north (Figure 1). The convergence of the seawater $\varepsilon_{Nd}(t)$ values between Sites 323 and 596, as well as the deep water and southerly locations of the two sites, suggests that both were influenced by the same deep water mass from at least ~62 to ~57 Ma (and likely to at least ~33 Ma; however, a hiatus at Site 323 limits the long-term correlation to Site 596). The relatively constant values recorded at Site 596 (situated at or below 4000 m depth throughout the study interval) suggest this water mass composition was a long-term feature of the southern Pacific. The average deep water $\varepsilon_{Nd}(t)$ values recorded at Sites 869, 865, and 463 were −4.7, −4.1, and −4.3, respectively, indicating a general geographic trend of increasing isotopic values from south to north (after Site 323 had subsided to deep water depths) (Figure 1 and Table S4 in the supporting information).

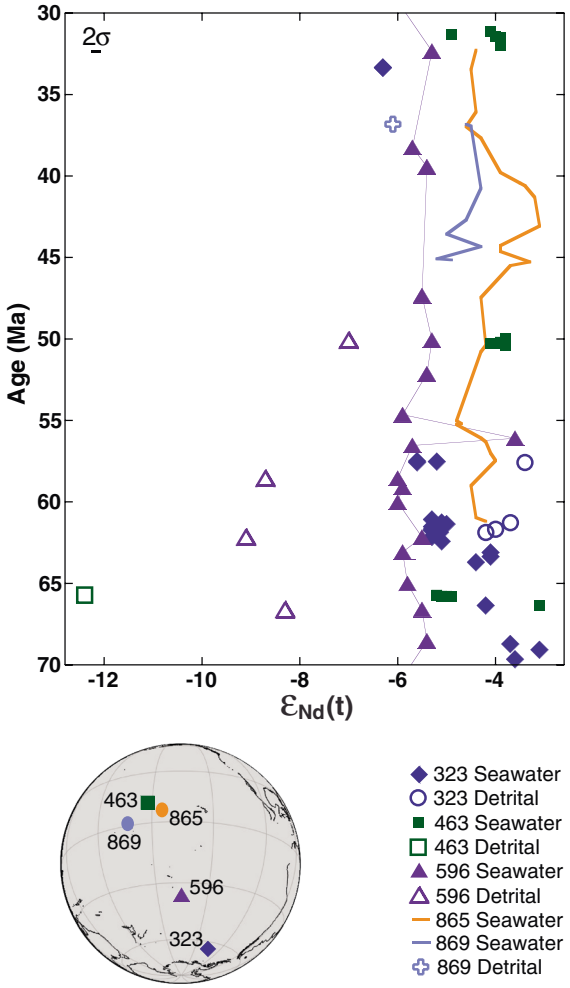

Figure 1. Pacific Ocean Nd isotope data from DSDP and ODP Sites 323, 463, 596, 865, and 869. Error bars for individual samples are smaller than the symbol size, and external precision is indicated by black bar. Paleolocations shown are for 50 Ma (generated with GPlates software).

Previous work from northern Pacific sites also identified a general increase in intermediate and deep water Nd isotope values from south to north (Figure 2) [*Hague et al.*, 2012]. North Pacific Nd isotope data combined with coupled model simulations indicate convection of a water mass with radiogenic Nd isotope values in the North Pacific and circulation of this water mass southward [*Thomas*, 2004; *Hague et al.*, 2012]. The systematic decrease in the deep water Nd isotope composition indicated by the data compilation could have resulted from a combination of (1) boundary exchange along the western margin of the Pacific with less radiogenic seafloor sediments and (2) mixing with a water mass of lower isotopic composition that convected in the southern Pacific. Although fine-grained detrital sediments in the tropical and subtropical Pacific record relatively low Nd isotope values, we rule out significant influence of dust dissolution on the deep water Nd isotope signature based on the overall low fluxes of dust to the region [*Woodard et al.*, 2011] and the negligible exchange of Nd between silicate dust and seawater [*Jones et al.*, 1994]. Boundary exchange, defined as exchange of Nd between seafloor sediments and the advecting water mass [*Lacan and Jeandel*, 2005], may have contributed to the overall decrease in the isotopic composition of North Pacific Deep Waters. However, much of the western margin of the North Pacific during the Late Cretaceous and Paleogene was characterized by subduction [e.g., *Seton et al.*, 2012], and thus, detrital sediments deposited along the margin likely recorded relatively high Nd isotope values. Boundary exchange alone cannot explain the geographic pattern of decreasing isotopic composition to the south.

To constrain the source(s) of Nd to the tropical and South Pacific and test the hypothesis that a water mass of relatively low Nd isotopic composition convected in the region, we analyzed the Nd isotopic composition of targeted detrital sediments (Figure 1 and Table S4 in the supporting information). Fluvial inputs of weathered rock are the dominant source of dissolved Nd to the oceans, and fine-grained detrital sediments transported by rivers bear the same Nd isotopic composition as the dissolved inventory [*Goldstein et al.*, 1984; *Goldstein and Jacobsen*, 1987, 1988]. However, the only source of detrital sediments to sites located far from land (>2000 km) is windblown dust and ash [*Rea*, 1994]. Sites 463, 596, and 869 were all located toward the center of the basin (Figure 1), and the range of detrital $\varepsilon_{Nd}(t)$ values recorded at those sites (−6.1 to −12.4) is consistent with contributions from continental dust and volcanic ash. Furthermore, the detrital $\varepsilon_{Nd}(t)$ values at Sites 463, 596, and 869 are all lower than the seawater values recorded at those sites (Figure 1), indicating that the sources of the detrital sediments were different than those of the water masses at Sites 463, 596, and 869. Site 323, situated near the Antarctic Peninsula, recorded the most radiogenic detrital silicate $\varepsilon_{Nd}(t)$ values (−3.4 to −4.0; Figure 1). Subduction of the proto-Pacific plates during the Mesozoic and Cenozoic produced the peninsula [*Barker*, 1982], and $\varepsilon_{Nd}(t)$ values of the exposed terranes ranges from ~ −6 to ~ +5 [*Wareham et al.*, 1997;

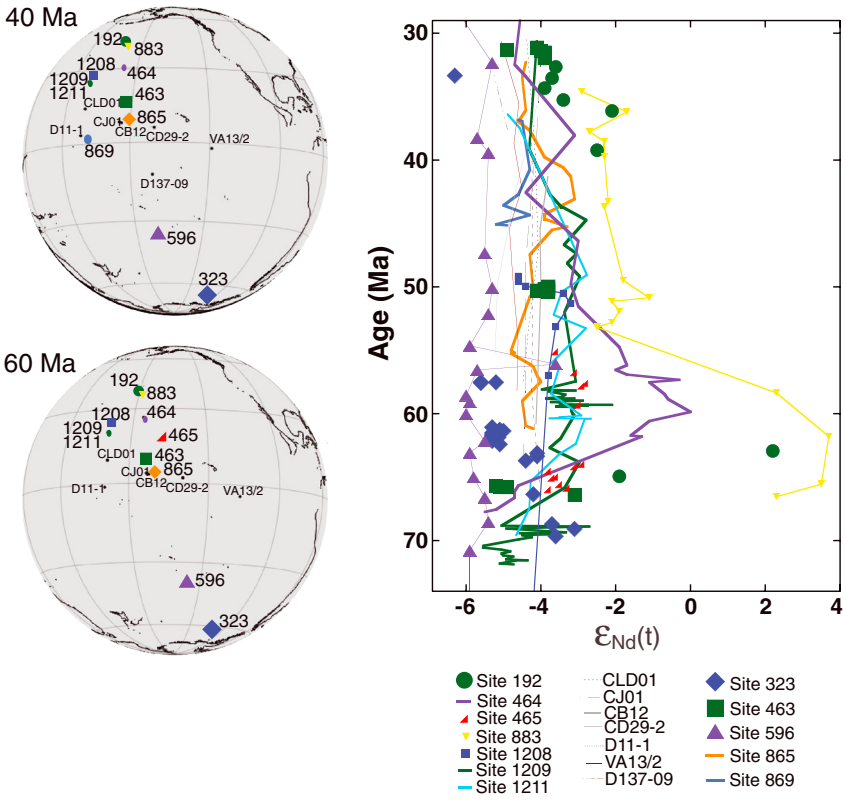

Figure 2. Compilation of new (Sites 323, 463, 596, 865, and 869) with representative published data from the North and tropical Pacific. Crusts CD 29–2, D11-1, VA13/2 [*Ling et al.*, 1997]; Sites 1209 and 1211 [*Thomas*, 2004]; Crust D137-09 [*van de Flierdt et al.*, 2004]; Crusts CB01, CJ01, and CLD01 [*Ling et al.*, 2005]; and Sites 192, 464, 465, 883, and 1208 [*Hague et al.*, 2012]. Paleolocations shown are for 60 and 40 Ma (from GPlates).

Riley et al., 2001]. The Site 323 detrital silicate $\varepsilon_{Nd}(t)$ values are consistent with a mixture of Antarctic Peninsula weathering inputs with the above range of $\varepsilon_{Nd}(t)$ values. Given the proximity of Site 323 to the continental margin, the dissolved fluvial inputs (and hence sea surface composition) would have been similar to the detrital composition.

The key features in the compilation of data shown in Figure 2 are (1) the convergence of seawater $\varepsilon_{Nd}(t)$ values at Sites 323 and 596 coincident with deepening at Site 323, (2) the general northerly increase in the seawater $\varepsilon_{Nd}(t)$ values post deepening at Site 323, (3) the consistency of Site 596 deep water $\varepsilon_{Nd}(t)$ values, and (4) the decoupling of dissolved and detrital values at Sites 463, 596, and 869. These features exhibited by the data are best explained by convection of deep waters in the Pacific sector of the Southern Ocean that flowed northward and mixed with radiogenic deep waters that convected in the North Pacific. Boundary exchange with a northward flowing South Pacific water mass cannot account for the systematic increase in the deep water Nd isotope composition because the likely composition of detrital sediments along the western margin of the South Pacific was relatively low based on tectonic considerations. Initiation of subduction in the subtropical and tropical regions of the west Pacific did not occur until ~50 Ma [e.g., *Seton et al.*, 2012], and prior to the weathering of the subduction-related terranes the marginal sediments in the region would have had a relatively low Nd isotopic composition.

The relatively radiogenic signature of the Southern Ocean source is unique to the Pacific sector, because the Atlantic and Indian sectors recorded significantly lower $\varepsilon_{Nd}(t)$ values during the Late Cretaceous and early Paleogene [*Thomas et al.*, 2003; *Robinson et al.*, 2010; *Murphy and Thomas*, 2012]. We adopt the name "South Pacific Deep Water" (SPDW) to distinguish the Pacific sector source from the other Southern Ocean sectors and "North Pacific Deep Water" (NPDW) to identify the water mass from the north. The vertical $\varepsilon_{Nd}(t)$ section based on a compilation of available data (Figure 3) reveals deep penetration of the NPDW and SPDW signals and the creation of a broad intermediate water mass between them. Furthermore, the available data delineate a

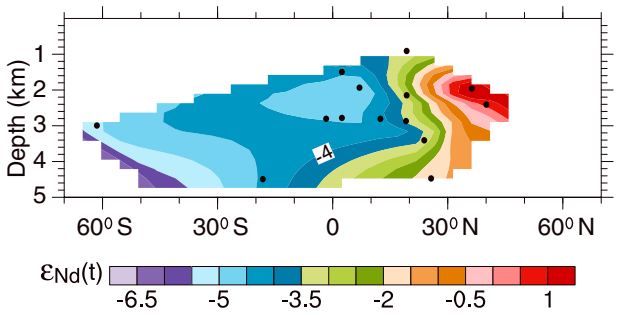

Figure 3. Compilation of $\varepsilon_{Nd}(t)$ records for the Pacific for 67–53 Ma interpolated using natural neighbor interpolation (Please refer to the supporting information for the data used in the compilation). Data are plotted at their 60 Ma paleopositions and paleodepths (dots indicate core paleopositions).

prominent "front" at ~30°N that extends throughout much of the water column. The geographic and vertical distribution of $\varepsilon_{Nd}(t)$ suggests a bipolar convection mode, and the homogenous region of SPDW-influenced values indicates a mixing zone substantial in latitudinal and vertical extent. The lower $\varepsilon_{Nd}(t)$ values, representing the core of SPDW, extend deeper and further northward than the corresponding NPDW feature indicating that this water was denser than its northern counterpart. Between 2 and 3 km water depth the $\varepsilon_{Nd}(t)$ compilation reveals a tongue of more negative $\varepsilon_{Nd}(t)$ values impinging on the equator indicating that three-dimensional aspects of the circulation are important and potentially a key diagnostic feature.

We propose that SPDW convection occurred in the Ross Sea, which extended further south than other portions of the Southern Ocean, and is supported by evidence of Paleocene age sediment drifts in the Amundsen Sea [*Uenzelmann-Neben and Gohl*, 2012]. The end-member SPDW composition represented by the convergence of Sites 323 and 596 values between ~ −5.0 and −5.6 indicates mixing of Antarctic Peninsula weathering inputs with other source(s) of more unradiogenic surface water Nd in the Ross Sea region prior to convection, either through weathering of older Antarctic terranes [*Roy et al.*, 2007] and/or surface water transport of unradiogenic Nd from the proto-Indian region [*Murphy and Thomas*, 2012].

The $\varepsilon_{Nd}(t)$ compilation also indicates distinct Pacific and Atlantic overturning circulations that remained separate until at least ~40 Ma, when SPDW values converged with those recorded in the Atlantic sector of the Southern Ocean [*Scher and Martin*, 2004]. The separation of the deep Atlantic and Pacific during the early Cenozoic has important implications for carbon cycling: multiple sources of deep convection would have produced a distribution of younger water mass ages in each basin and overall faster rates of ventilation. Higher ventilation rates promote enhanced recycling of organic carbon, returning the fixed carbon back to the ocean/atmosphere system as CO_2 [*Olivarez Lyle and Lyle*, 2006; *Hague et al.*, 2012]. Equally important, the segregation at depth of the relatively small Atlantic from the much larger Pacific explains the differential responses to increased levels of atmospheric CO_2 during the Paleogene hyperthermals [*Zeebe and Zachos*, 2007], since a finite mass of CO_2 equilibrated in the small Atlantic would cause more dissolution than in the Pacific. The global compilation also demonstrates a lack of a tropical east-west $\varepsilon_{Nd}(t)$ gradient, indicating that deep water exchange through the open Caribbean and Tethys was insignificant [*Thomas et al.*, 2008].

3.2. Model Simulations

To evaluate the proxy interpretations in a physical oceanographic context, we performed a suite of Nd tracer-enabled simulations with the MIT general circulation model (MITgcm) using early Paleogene continental configuration, surface boundary conditions appropriate to the period, and a variety of vertical-mixing profiles (Figure 4). Boundary conditions were taken from two sets of previously coupled experiments whose resulting surface temperatures compare favorably with proxy reconstructions from the middle and late Eocene and Paleocene [*Liu et al.*, 2009; *Hollis et al.*, 2009, 2012; *Ali and Huber*, 2010; *Huber*, 2009] in one case and the warmer early Eocene in the other [*Huber and Caballero*, 2011; *Lunt et al.*, 2012]. The boundary conditions are taken from the set of fully coupled experiments described in *Liu et al.* [2009] and *Huber and Caballero* [2011] using version 3 of the Community Climate System Model (CCSM3) and forced with elevated CO_2, lower than present-day aerosol concentrations, and paleogeography of *Sewell et al.* [2000]. The warm boundary conditions are from the coupled experiments using 8 times preindustrial era CO_2 (2240 ppm) while the very warm ones come from the experiments with 16 times preindustrial levels (4480 ppm). These levels ought not be treated literally: note that CCSM3 has a lower climate sensitivity to elevated CO2 than the ensemble mean of general circulation models considered by the Intergovernmental Panel on Climate Change, which means that the same

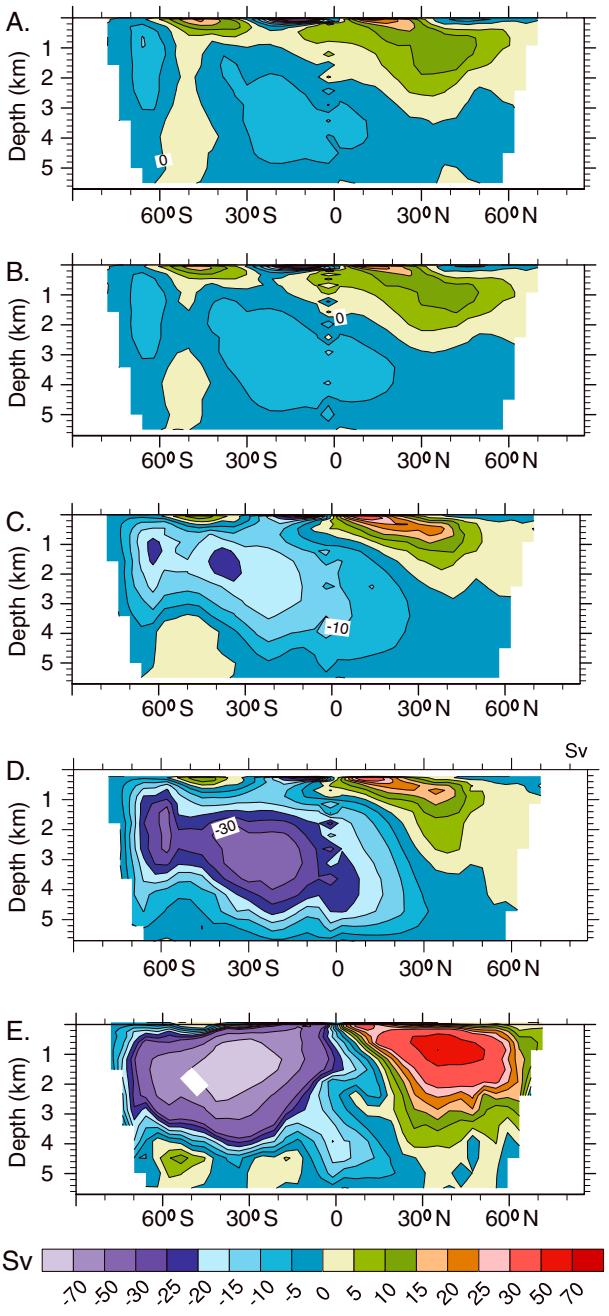

Figure 4. The global meridional overturning stream function for the Pacific reconstructions plotted (S_v), with negative values indicating counterclockwise flow. (a) Results of normal mixing applied to the warm simulation. (b) Normal mixing applied to the very warm simulation. (c) Moderate mixing in the very warm simulation. (d) Strong abyssal mixing in the very warm simulation. (e) Strong mixing for the very warm simulation.

degree of surface warming could be achieved using lower concentrations of CO_2 than required by CCSM3 in different model with a higher sensitivity.

Iterations of the very warm coupled experiments were repeated using three different ocean mixing profiles shown in Figure 5. These feature normal (i.e., present day), moderate (higher), and strong (much higher) vertical diffusivity. The vertical diffusivity used "normal mixing" cases follows a Bryan-Lewis type profile [*Bryan and Lewis*, 1979] that transitions from 0.1 cm^2/s in the upper ocean to higher values in the abyss (1.0 cm^2/s) beginning around a depth of 1 km; this is similar to estimates of diffusivity values for the modern ocean. Two profiles with values 0.5 cm^2/s and 4.7 cm^2/s larger at all depths ("moderate mixing" and "strong mixing," respectively) were also tested with the very warm conditions. These three coupled runs, combined with the warm case using normal mixing, yield four unique sets of boundary conditions; we applied them to the MITgcm in ocean-only mode [*Marshall et al.*, 1997], which generated the Nd tracer distributions presented here.

To further explore the effects of mixing profiles, several additional tests tethering strong abyssal diffusivity to weak upper ocean profiles were run in the ocean-only MITgcm; we present one of these here ("strong abyssal mixing"). Because there is no counterpart to this simulation in the fully coupled model, the choice of which boundary conditions to apply must be considered. We tested each set of boundary conditions with the strong abyssal mixing profile and found that the northward ocean heat transport was similar to the one with moderate mixing, so we adopted the surface boundary conditions from the moderate mixing case for the strong abyssal mixing case as well. It is important to note that we explored the parameter space using other combinations of boundary conditions and profiles, and the resulting Nd tracer distributions in these cases were qualitatively similar to those we report here.

Deep water forms at both the northern and southern end of the Pacific in all of the cases we examined, but the strength and structure of the Pacific meridional overturning circulation differ with the vertical-mixing profile. Using the normal mixing (i.e., present-day profiles) with either warm boundary conditions (Figure 4a)

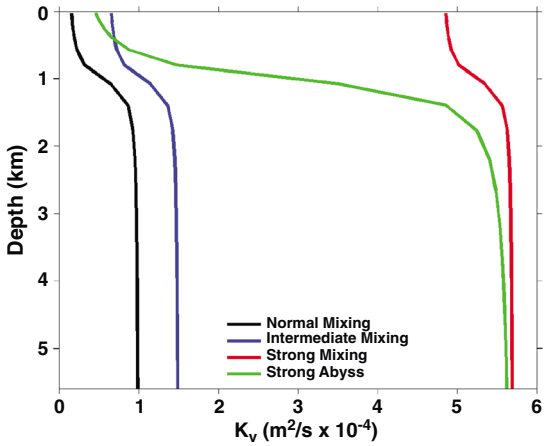

Figure 5. Vertical diffusivity profiles for the four simulated mixing cases (normal, moderate, strong, and strong abyssal).

or very warm (Figure 4b) yields a circulation with North Pacific deep water to depths of about 2.5 km in the Northern Hemisphere, with water sinking in the Southern Hemisphere filling depths below and points southward. This indicates that deep water forms at both the northern and southern end of the Pacific in simulations with both warm (Figure 4a) and very warm boundary conditions (Figure 4b), showing that bipolar modes of sinking can occur when forced with boundary conditions for both the very warm early Eocene as well as those more representative of the cooler Paleocene and middle to late Eocene. Yet the strength and structure of the Pacific circulation vary with the strength of the mixing imposed, which has implications for the expected distribution of tracers in the tropical Pacific. Below we describe the responses to various vertical-mixing profiles.

Increasing mixing by 0.5 cm^2/s to the levels in the moderate mixing case (and applying the set of boundary conditions from the corresponding fully coupled run) yields a stronger overturning and more dominant Southern Hemisphere source (Figure 4c). Further amplifying mixing values to levels of the strong abyssal mixing (Figure 4d) or strong mixing cases (Figure 4e) strengthens the overturning further while maintaining a bimodal structure of sinking at both the northern and southern end of the Pacific. The elevated mixing profiles affect the ocean heat transport, passive tracer distribution, surface temperature gradient, and energy consumed by mixing.

The best match with the reconstructed proxy distribution occurs in the cases using mixing values stronger than those of present day. The moderate mixing case (which adds 0.5 cm^2/s to the normal mixing profile), the strong mixing case (which adds an additional 4.2 cm^2/s to the moderate profile), and the strong abyssal mixing (which marries the strong mixing values below 1 km depth to weaker surface ones) produce a gradient across the tropical Pacific between water with Southern Hemispheric imprints and Northern Hemispheric origins (Figure 6). The best match with the proxy data (Figure 3 and shown again in Figure 6f) occurs in cases using the strongest abyssal mixing (Figures 6d and 6e), although the moderate mixing (Figure 6c) also shows some qualitative improvements to the proxy comparison over the normal mixing cases (Figures 6a and 6b), which simulate strong vertical gradients in Nd values through the tropical Pacific. Note that both the strong mixing and strong abyssal mixing, whose diffusivity values differ principally only in the upper ocean, compare favorably with the proxy data, indicating a lack of sensitivity to upper ocean mixing values.

While the match between proxy and model Nd tracer distributions was unaffected by upper ocean diffusivities, the ocean heat transport and surface temperatures were strongly affected by the strength of mixing in the thermocline. Figure 7a shows the ocean heat transport in the MITgcm using normal (black), moderate (blue), and strong (red) mixing profiles. Elevated mixing increases the poleward heat transport carried by the ocean, with the highest sensitivity to mixing occurring in the tropical thermocline [e.g., *Bugnion et al.*, 2006]. We found further evidence of this localized sensitivity in that the ocean heat transport in simulations using strong abyssal mixing profile were similar to those using moderate mixing rather than strong mixing. The strong abyssal mixing profile is similar to that of the moderate cases only in the upper most 700 m of the ocean. These mixing profiles change the meridional sea surface temperature distribution simulated in the coupled model, as shown in Figure 7b. The case using strong mixing produces the weakest gradient and best match with high-latitude proxies.

Given that the best match between proxy and model-derived Nd cross sections occurred in simulations using elevated mixing, we examine here how much energy would be required to maintain these stronger profiles. Following *Wunsch and Ferrari* [2004], we calculated the amount of energy required by mixing processes by

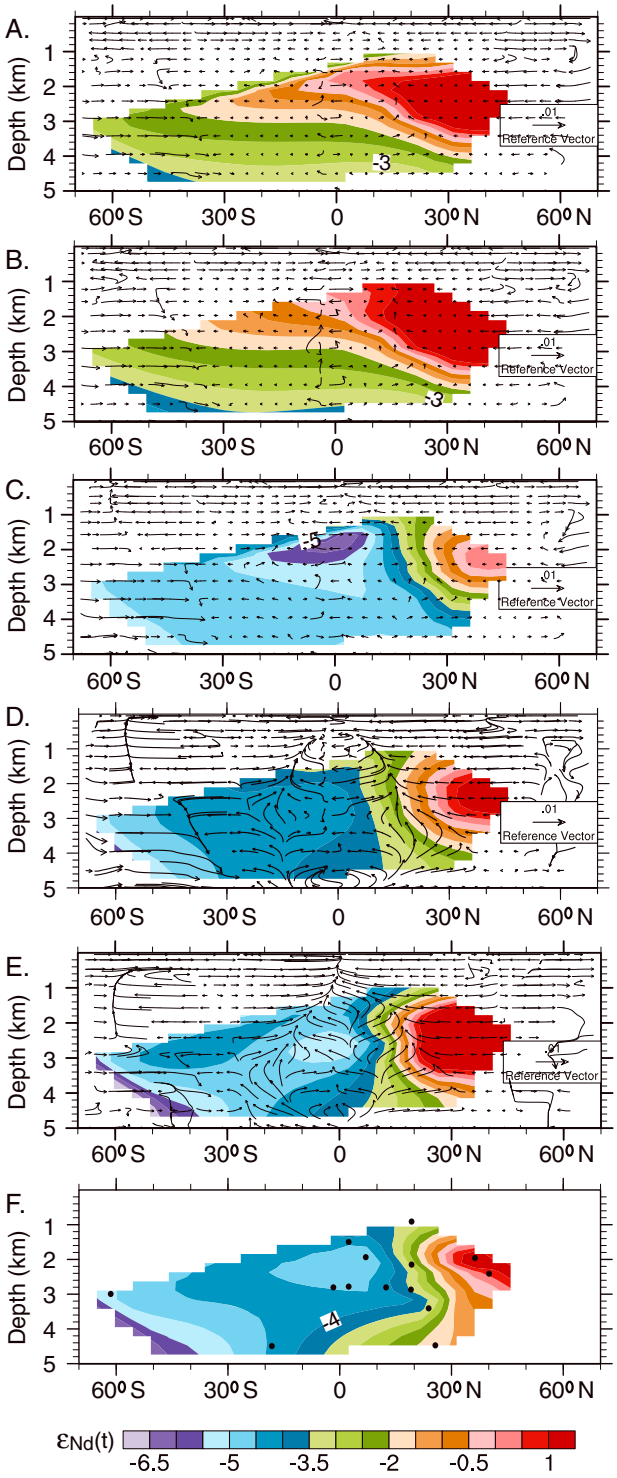

Figure 6. (a) Results of normal mixing applied to the warm simulation. (b) Normal mixing applied to the very warm simulation. (c) Moderate mixing in the very warm simulation. (d) Strong abyssal mixing in the very warm simulation. (e) Strong mixing for the very warm simulation. (f) Compilation of $\varepsilon_{Nd}(t)$ records for the Pacific interpolated using natural neighbor interpolation. Data are plotted at their 60 Ma paleopositions and paleodepths (dots indicate core paleopositions). In Figures 6a–6e, model-derived vertical and meridional velocity vectors (m/s) in a transect through the paleo-Pacific are overlain on model-predicted $\varepsilon_{Nd}(t)$ values that are plotted using the same geographic sampling as in the compilation in Figure 6f. Vertical velocities have been multiplied by $1x10^4$ for clarity.

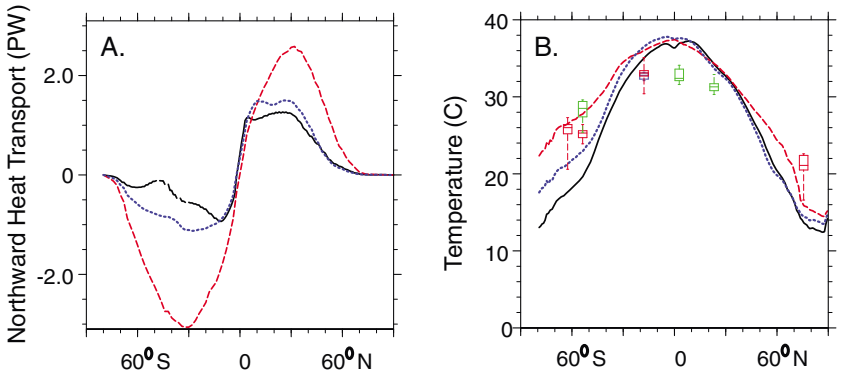

Figure 7. (a) The zonal mean meridional heat transport in PW produced by CCSM3 for the normal (black line), moderate (blue line), and strong (red line) mixing cases. (b) Sea surface temperatures averaged across the Pacific for the same three cases compared with a compilation of early Eocene sea surface temperatures. The box-whisker plots represent median, 95 and 5% confidence intervals, and maximum and minimum values for TEX_{86} (red), Mg/Ca (green), and glassy foraminiferal $\delta^{18}O$ (blue) annual mean surface temperature estimates (Table S3).

integrating the product of the vertical diffusivity K_v and the square of the Brunt-Väisälä frequency N over the volume of the model ocean:

$$\varepsilon = \Gamma \int K_v N^2 \rho \, dV$$

The integral is the fraction of the dissipation available to actually mix the fluid; it is related to the total viscous dissipation ε by a so-called mixing efficiency Γ, which is estimated to be about 0.2 in the modern ocean [e.g., *Wunsch and Ferrari*, 2004]. Absent knowledge of how such a parameter might differ over geologic time, we use the value 0.2 in all of our calculations.

Under these assumptions, the normal mixing case would require a source of 1.41 TW, while the moderate mixing case requires a larger one of 4.32 TW. The strong abyssal mixing case requires 5.49 TW and the strong mixing case requires 20.93 TW. It is important to note that the estimate of the energy required is most sensitive to elevated mixing in the upper kilometer, while the Nd profiles are not. The closest matches between data and proxies are achieved with elevated mixing in the abyss, regardless of whether values in the upper ocean are elevated to high values. On the other hand, the best match with surface temperature proxies occurs when mixing is elevated in the upper ocean, but achieving this requires an implied source of energy nearly an order of magnitude larger than that input to the oceans today.

The estimated size of the energy source required for moderate mixing and strong abyssal mixing simulations is within a factor of 2 to 3 of that available today. One potential source for such an increase is (for abyssal mixing) tidal dissipation. Though much of the present-day tide is dissipated on shelves, *Green and Huber* [2013] argued that an increase in dissipation in the deep paleo-Pacific during the Eocene would result from the changes in continental geography. They found that 94% of the Pacific tidal energy is lost in the deep part of the basin using Eocene geography and conditions, while only 45% is with present geography and conditions. Even while the global dissipation was lower in the Eocene simulations compared to today, the absolute amount dissipated in the abyssal Pacific increased from ~0.9 to ~1.2 TW (note that this is an actual amount of dissipated energy, not an estimate of energy available for mixing processes; global amounts of the former are assumed to be related to global amounts of the latter by the mixing efficiency factor $\Gamma \sim 0.2$).

While substantially elevated mixing in the upper ocean (strong mixing case) does not appear necessary for good agreement between model and proxy Nd cross sections, it does improve agreement with other proxies of surface temperatures. Yet raising the diffusivity this high in the upper kilometer presents a new problem in that the source of energy would have to rise substantially beyond that available today (unless some other mechanisms favored a larger value for the mixing efficiency parameter in the Paleogene). One potential source of energy for mixing at these depths, particularly in low latitudes where poleward heat transport is most sensitive to mixing [*Bugnion et al.*, 2006], is strong surface winds from severe storms. Increases in tropical cyclone wind forcing could result in additional mixing at these depths in hot climates [*Korty et al.*, 2008], and mixing from transient wind bursts has been documented to have a strong effect [*Wijesekera and*

Gregg, 1996]. While several models of storm activity in a warmer climate predict an increase in high-intensity storms and of the cumulative power put into the upper ocean by these strong tropical cyclone winds [e.g., *Fedorov et al.*, 2009; *Bender et al.*, 2010], the way these storms respond to climate differences as large as those of the early Cenozoic is unclear.

3.3. Potential Implications

The model-data synthesis confirms the qualitative interpretation of the proxy records that bipolar convection operated in the Pacific during the latest Cretaceous and early Paleogene, and permits us to quantitatively explore the implications of the MOC reconstruction. One important feature that emerges from the proxy data and simulations is that the mode of overturning circulation did not respond to major transitions in early Cenozoic climate. Bipolar Pacific convection dominated by SPDW characterized both the warm (2240 ppm atmospheric CO_2 forcing) and very warm (4480 ppm CO_2 forcing) simulations. The proxy compilation (Figure 2) and simulations with normal background vertical diffusivity (Figures 6b and 6c) suggest a weak feedback between ocean circulation and climate. The sensitivity of climate state to MOC increases dramatically with increased simulated vertical mixing. Enhanced abyssal mixing requires approximately 1 TW of energy for moderate and strong abyssal mixing cases and could have occurred in the past because of enhanced abyssal tidal dissipation [*Kagan and Sündermann*, 1996; *St. Laurent et al.*, 2002; *Green and Huber*, 2013], greater interaction of wind-driven internal wave activity with submarine plateaus, or higher than modern values of the geothermal heat flux [*Emile-Geay and Madec*, 2009]. It is likely that some combination of all of these processes contributed to enhanced abyssal mixing given that each would have been promoted by the tectonic boundary conditions specific to the Late Cretaceous and early Paleogene. The widespread emplacement of large igneous provinces and high rates of oceanic crust production contributed to significantly higher fluxes of heat through enhanced water/rock interaction. At the same time, high rates of crustal emplacement via mid-ocean ridge or plume volcanism produced significant regions of relatively young and buoyant (shallower) seafloor. Alternatively, this mixing may arise in the absence of stronger mechanical forcing as a consequence of a static stability dependence of mixing rates [*Nilsson et al.*, 2003].

Stronger vertical mixing within the oceans potentially reconciles several long-standing greenhouse paleoclimate problems. Stronger vertical mixing invigorates the MOC by an order of magnitude (Figures 4c–4e compared with Figures 4a and 4b), increases ocean heat transport by 50–100% (Figure 7a), reduces the zonal mean equator-to-pole temperature gradients by up to 6°C (Figure 7b), lowers tropical peak terrestrial temperatures by up to 6°C, and warms high-latitude oceans by up to 10°C (Figure 7b). These features are all consistent with the recent proxy temperature reconstructions [*Hollis et al.*, 2009]. The redistribution of heat is rectified by the positive high-latitude water vapor and albedo feedbacks in the model [*Abbot et al.*, 2009] to produce significant increases (~2°C) in global mean temperature, comparable to a doubling of CO_2. This rectification may be an important process rendering past greenhouse climates warmer than predicted based on consideration of greenhouse gases alone [*Pagani et al.*, 2006; *Liu et al.*, 2009; *Hollis et al.*, 2012].

4. Conclusions

Nd isotope data from South Pacific Deep Sea Drilling Project (DSDP) and Ocean Drilling Program (ODP) Sites 323, 463, 596, 865, and 869 provide new evidence for deep convection in the South Pacific during the latest Cretaceous through early Paleogene (~70 to 30 Ma). Compilation with previously published data confirms a bipolar mode of convection in the Pacific that was separated from Atlantic meridional overturning circulation until at least ~40 Ma. Numerical simulations independently confirm the existence of a vigorously circulating ocean with multiple deep convection sites. The best data-model match is achieved with strong oceanic vertical mixing, particularly in the abyssal ocean. Strong abyssal mixing likely was a consequence of tidal mixing, internal wave interactions, and heat flow associated with Late Cretaceous and early Paleogene tectonic processes that produced significant regions of relatively young and buoyant (shallower) seafloor. The simulated and proxy-reconstructed MOC is consistent with geologic evidence for well-ventilated Paleogene oceans, low meridional temperature gradients, and high global mean temperatures.

Acknowledgments
This work was funded by NSF ATM 0927769 to D.J.T., and R.K. and NSF-ATM 0927946 to M.H. J.S. received support from NSF S-STEM 0806926. Samples were provided by the Integrated Ocean Drilling Program and analyzed in the R. Ken Williams '45 Radiogenic Isotope Geosciences Laboratory. We thank the reviewers and editor for their thoughtful comments.

References

Abbot, D. S., M. Huber, G. Bousquet, and C. C. Walker (2009), High-CO_2 cloud radiative forcing feedback over both land and ocean in a global climate model, *Geophys. Res. Lett.*, *36*, L05702, doi:10.1029/2008GL036703.

Ali, J., and M. Huber (2010), Mammalian biodiversity on Madagascar controlled by ocean currents, *Nature*, *463*, 653–656.
Amakawa, H., D. S. Alibo, and Y. Nozaki (2000), Nd isotopic composition and REE pattern in the surface waters of the eastern Indian Ocean and its adjacent seas, *Geochim. Cosmochim. Acta*, *64*, 1715–1727.
Amakawa, H., K. Sasaki, and M. Ebihara (2009), Nd isotopic composition in the central North Pacific, *Geochim. Cosmochim. Acta*, *73*, 4705–4719.
Arthur, M. A., S. O. Schlanger, and H. C. Jenkyns (1987), The Cenomanian-Turonian oceanic anoxia event: II. Paleoceanographic controls on organic matter production and preservation, in *Marine and Petroleum Source Rocks*, edited by J. Brooks and A. J. Fleet, *Geol. Soc. London Spec Publ.*, *26*, 401–420.
Arzouse, T., J.-C. Dutay, F. Lacan, and C. Jeandel (2007), Modeling the neodymium isotopic composition with a global ocean circulation model, *Chem. Geol.*, *239*, 165–177.
Barker, P. F. (1982), The Cenozoic subduction history of the Pacific margin of the Antarctic Peninsula: Ridge crest-trench interactions, *J. Geol. Soc. London*, *139*, 787–801.
Barrera, E., S. M. Savin, E. Thomas, and C. E. Jones (1997), Evidence for thermohaline-circulation reversals controlled by sea-level change in the latest Cretaceous, *Geology*, *25*, 715–718.
Bender, M. A., T. R. Knutson, R. E. Tuleya, J. J. Sirutis, G. A. Vecchi, S. T. Garner, and I. M. Held (2010), Modeled impact of anthropogenic warming on the frequency of intense Atlantic hurricanes, *Science*, *327*, 454–458.
Bralower, T. J., J. C. Zachos, E. Thomas, M. Parrow, C. K. Paull, D. C. Kelly, I. Premoli Silva, W. V. Sliter, and K. C. Lohmann (1995), Late Paleocene to Eocene paleoceanography of the equatorial Pacific Ocean: Stable isotopes recorded at Ocean Drilling Program Site 865, Allison Guyot, *Paleoceanography*, *10*, 841–865, doi:10.1029/95PA01143.
Bryan, K., and L. J. Lewis (1979), A water mass model of the world ocean, *J. Geophys. Res.*, *84*(C5), 2503–2517, doi:10.1029/JC084iC05p02503.
Bugnion, V., C. Hill, and P. H. Stone (2006), An adjoint analysis of the meridional overturning circulation in an ocean model, *J. Clim.*, *19*, 3752–3750.
Carter, P., D. Vance, C. D. Hillenbrand, J. A. Smith, and D. R. Shoosmith (2012), The neodymium isotopic composition of water masses in the eastern Pacific sector of the Southern Ocean, *Geochim. Cosmochim. Acta*, *79*, 41–59.
DePaolo, D. J., and G. J. Wasserburg (1976), Nd isotopic variations and petrogenetic models, *Geophys. Res. Lett.*, *3*, 249–252, doi:10.1029/GL003i005p00249.
Elderfield, H. R., J. Upstill-Goddard, and E. R. Sholkolvitz (1990), The rare earth elements in rivers, estuaries, and coastal seas and their significance to the composition of ocean waters, *Geochim. Cosmochim. Acta*, *54*, 971–991.
Emile-Geay, J., and G. Madec (2009), Geothermal heating, diapycnal mixing and the abyssal circulation, *Ocean Sci.*, *5*, 203–217.
Fedorov, A. V., C. M. Brierley, and K. Emanuel (2009), Tropical cyclones and permanent El Niño in the early Pliocene epoch, *Nature*, *463*, 1066–1070.
Firth, J. V. (1995), Data report: Cenozoic calcareous nannofossils of Hole 869A, equatorial Pacific Ocean, in *Proceedings of the Ocean Drilling Program, Sci. Results*, vol. 143, edited by E. L. Winterer et al., pp. 567–570, Ocean Drilling Program, College Station, Tex.
Frank, M. (2002), Radiogenic isotopes: Tracers of past ocean circulation and erosional input, *Rev. Geophys.*, *40*(1), 1001, doi:10.1029/2000RG000094.
Goldstein, S. J., and S. B. Jacobsen (1987), The Nd and Sr isotopic systematics of river water dissolved material: Implications for the sources of Nd and Sr in seawater, *Chem. Geol.*, *66*, 245–272.
Goldstein, S. J., and S. B. Jacobsen (1988), Nd and Sr isotope systematics of river water suspended material: Implications for crustal evolution, *Earth Planet. Sci. Lett.*, *87*, 249–265.
Goldstein, S. J., R. K. O'Nions, and P. J. Hamilton (1984), A Sm-Nd isotopic study of atmospheric dusts and particulates from major river systems, *Earth Planet. Sci. Lett.*, *70*, 221–236.
Gradstein, F. M., J. G. Ogg, and A. B. Smith (2005), *A Geological Time Scale 2004*, 610 pp., Cambridge Univ. Press, Cambridge, U. K.
Green, J. A. M., and M. Huber (2013), Tidal dissipation in the early Eocene and implications for ocean mixing, *Geophys. Res. Lett.*, *40*, 2707–2713, doi:10.1002/grl.50510.
Hague, A. M., D. J. Thomas, M. Huber, R. Korty, S. Woodard, and L. B. Jones (2012), Convection of North Pacific deep water during the early Cenozoic, *Geology*, *40*, 527–530, doi:10.1130/G32886.1.
Halliday, A. N., J. P. Davidson, P. Holden, R. M. Owen, and A. M. Olivarez (1992), Metalliferous sediments and the scavenging residence time of Nd near hydrothermal vents, *Geophys. Res. Lett.*, *19*, 761–764, doi:10.1029/92GL00393.
Hollis, C. J., et al. (2009), Tropical sea temperatures in the high-latitude South Pacific during the Eocene, *Geology*, *37*, 99–102.
Hollis, C. J., et al. (2012), Early Paleogene temperature history of the southwest Pacific Ocean: Reconciling proxies and models, *Earth Planet. Sci. Lett.*, *349–350*, 53–66.
Hollister, C. D., et al. (1976), *Initial Reports of the Deep Sea Drilling Project*, vol. 35, 930 pp., U.S. Government Printing Office, Washington, D. C.
Huber, M. (2009), Snakes tell torrid tale, *Nature*, *457*, 669–671.
Huber, M., and R. Caballero (2011), The early Eocene equable climate problem revisited, *Clim. Past*, *7*, 603–633.
Huber, M., and L. C. Sloan (2001), Heat transport, deep waters, and thermal gradients: Coupled simulation of an Eocene greenhouse climate, *Geophys. Res. Lett.*, *28*, 3481–3484, doi:10.1029/2001GL012943.
Jeandel, C. (1993), Concentration and isotopic composition of Nd in the South Atlantic Ocean, *Earth Planet. Sci. Lett.*, *117*, 581–591.
Jeandel, C., D. Thouron, and M. Fieux (1998), Concentration and Atlantic isotopic compositions of neodymium in the eastern Indian Ocean and Indonesian straits, *Geochim. Cosmochim. Acta*, *62*, 2597–2607.
Jones, C. E., A. N. Halliday, D. K. Rea, and R. M. Owen (1994), Neodymium isotopic variations in the North Pacific modern silicate sediment and the insignificance of detrital REE contributions to seawater, *Earth Planet. Sci. Lett.*, *127*, 55–66.
Kagan, B. A., and J. Sündermann (1996), Dissipation of tidal energy, paleotides, and evolution of the Earth-Moon system, *Adv. Geophys.*, *38*, 179–266.
Korty, R. L., K. A. Emanuel, and J. R. Scott (2008), Tropical cyclone-induced ocean mixing and climate: Application to equable climates, *J. Clim.*, *21*, 638–654.
Lacan, F., and C. Jeandel (2001), Tracing Papua New Guinea imprint on the central Equatorial Pacific Ocean using neodymium isotopic compositions and rare earth element patterns, *Earth Planet. Sci. Lett.*, *186*, 497–512.
Lacan, F., and C. Jeandel (2005), Neodymium isotopes as a new tool for quantifying exchange fluxes at the continent-ocean interface, *Earth Planet. Sci. Lett.*, *232*, 245–257.
Ling, H. F., K. W. Burton, R. K. O'Nions, B. S. Kamber, F. von Blanckenburg, A. J. Gibb, and J. R. Hein (1997), Evolution of Nd and Pb isotopes in central Pacific seawater from ferromanganese crusts, *Earth Planet. Sci. Lett.*, *146*, 1–12.
Ling, H. F., S.-Y. Jiang, M. Frank, H.-Y. Zhou, F. Zhou, Z.-L. Lu, X.-M. Chen, Y.-H. Jiang, and C.-D. Ge (2005), Differing controls over the Cenozoic Pb and Nd isotope evolution of deepwater in the central North Pacific Ocean, *Earth Planet. Sci. Lett.*, *232*, 345–361.

Liu, Z., M. Pagani, D. Zinniker, R. DeConto, M. Huber, H. Brinkhuis, S. R. Shah, R. M. Leckie, and A. Pearson (2009), Global cooling during the Eocene-Oligocene climate transition, *Science*, *323*, 1187–1190.
Lunt, D. J., et al. (2012), A model-data comparison for a multi-model ensemble of early Eocene atmosphere–ocean simulations: EoMIP, *Clim. Past*, *8*, 1229–1273, doi:10.5194/cpd-8-1229-2012.
Lyle, M. (1997), Could early Cenozoic thermohaline circulation have warmed the poles?, *Paleoceanography*, *12*, 161–167, doi:10.1029/96PA03330.
Marshall, J., A. Adcroft, C. Hill, L. Perelman, and C. Heisey (1997), A finite-volume, incompressible Navier Stokes model for studies of the ocean on parallel computers, *J. Geophys. Res.*, *102*, 5753–5756, doi:10.1029/96JC02775.
Martin, E. E., and B. A. Haley (2000), Fossil fish teeth as proxies for seawater Sr and Nd, *Geochim. Cosmochim. Acta*, *64*, 835–847.
Martin, E. E., and H. D. Scher (2004), Preservation of seawater Sr and Nd isotopes in fossil fish teeth: Bad news and good news, *Earth Planet. Sci. Lett.*, *220*, 25–39.
Martin, E. E., S. W. Blair, G. D. Kamenov, H. D. Scher, E. Bourbon, C. Basak, and D. N. Newkirk (2010), Extraction of Nd isotopes from bulk deep sea sediments for paleoceanographic studies on Cenozoic time scales, *Chem. Geol.*, *269*, 414–431.
Martin, E. E., K. G. MacLeod, A. Jimenez Berrocoso, and E. Bourbon (2012), Water mass circulation on Demerara Rise during the Late Cretaceous, *Earth Planet. Sci. Lett.*, *327–328*, 111–120.
McArthur, J. M., R. J. Howarth, and T. R. Bailey (2001), Strontium isotope stratigraphy: LOWESS version 3: Best fit to the marine Sr-isotope curve for 0–509 Ma and accompanying look-up table for deriving numerical age, *J. Geol.*, *109*, 155–170.
Murphy, D. P., and D. J. Thomas (2012), Middle Cretaceous deep-water formation in the Indian sector of the Southern Ocean, *Paleoceanography*, *27*, PA1211, doi:10.1029/2011PA002198.
Nilsson, J., G. Broström, and G. Walin (2003), The thermohaline circulation and vertical mixing: Does weaker density stratification give stronger overturning?, *J. Phys. Oceanogr.*, *33*, 2781–279.
Olivarez Lyle, A., and M. W. Lyle (2006), Missing organic carbon in Eocene marine sediments: Is metabolism the biological feedback that maintains end-member climates?, *Paleoceanography*, *21*, PA2007, doi:10.1029/2005PA001230.
Pagani, M., N. Pedentchouk, M. Huber, A. Sluijs, S. Schouten, H. Brinkhuis, J. S. Sinninghe Damste, G. R. Dickens, and Exp. 302 Scientists (2006), Arctic hydrology during global warming at the Palaeocene/Eocene thermal maximum, *Nature*, *442*, 671–675.
Piepgras, D. J., and S. B. Jacobsen (1988), The isotopic composition of neodymium in the North Pacific, *Geochim. Cosmochim. Acta*, *52*, 1373–1381.
Piepgras, D. J., and G. J. Wasserburg (1982), Isotopic composition of neodymium in waters from the Drake Passage, *Science*, *217*, 207–214.
Piepgras, D. J., and G. J. Wasserburg (1987), Rare earth element transport in the western North Atlantic inferred from Nd isotopic observations, *Geochim. Cosmochim. Acta*, *51*, 1257–1271.
Rea, D. K. (1994), The paleoclimatic record provided by eolian deposition in the deep sea—The geologic history of wind, *Rev. Geophys.*, *32*, 159–195, doi:10.1029/93RG03257.
Reynard, B., C. Lècuyer, and P. Grandjean (1999), Crystal-chemical controls on rare-earth element concentrations in fossil biogenic apatites and implications for paleoenvironmental reconstructions, *Chem. Geol.*, *155*, 233–241.
Riley, T., P. Leat, R. Pankhurst, and C. Harris (2001), Origins of large volume rhyolitic volcanism in the Antarctic Peninsula and Patagonia by crustal melting, *J. Petrol.*, *42*, 1043–1065.
Roberts, N. L., A. M. Piotrowski, J. F. McManus, and L. D. Keigwin (2010), Synchronous deglacial overturning and water mass source changes, *Science*, *327*, 75–78.
Robinson, S. A., D. P. Murphy, D. Vance, and D. J. Thomas (2010), Formation of 'Southern Component Water' in the Late Cretaceous: Evidence from Nd-isotopes, *Geology*, *38*, 871–874.
Rogl, F. (1976), Late Cretaceous to Pleistocene foraminifera from the southeast Pacific basin, DSDP Leg 35, in *Initial Reports of the Deep Sea Drilling Project*, vol. 35, pp. 539–555, U.S. Government Printing Office, Washington, D. C.
Roy, M., T. van de Flierdt, S. R. Hemming, and S. L. Goldstein (2007), $^{40}Ar/^{39}Ar$ ages of hornblende grains and bulk Sm/Nd isotopes of circum-Antarctic glacio-marine sediments: Implications for sediment provenance in the southern ocean, *Chem. Geol.*, *244*, 507–519.
Saenko, O. A. (2006), The effect of localized mixing on the ocean circulation and time-dependent climate change, *J. Phys. Oceanogr.*, *36*, 140–160.
Sager, W. W., et al. (1993), *Initial Reports of the Deep Sea Drilling Project*, vol. 143, Ocean Drilling Program, College Station, Tex.
Scher, H. D., and E. E. Martin (2004), Circulation in the Southern Ocean during the Paleogene inferred from neodymium isotopes, *Earth Planet. Sci. Lett.*, *228*, 391–405.
Seton, M., et al. (2012), Global continental and ocean basin reconstructions since 200 Ma, *Earth Sci. Rev.*, *113*, 212–270.
Sewell, J. O., L. C. Sloan, M. Huber, and S. Wing (2000), Climate sensitivity to changes in land surface characteristics, *Global Planet. Change*, *26*, 445–465.
Shaw, H. F., and G. J. Wasserburg (1985), Sm-Nd in marine carbonates and phosphates, *Geochim. Cosmochim. Acta*, *49*, 503–518.
Sholkovitz, E. R. (1993), The geochemistry of rare earth elements in the Amazon River estuary, *Geochim. Cosmochim. Acta*, *58*, 2181–2190.
Siddall, M., S. Khatiwala, T. de Flierdt, K. Jones, S. L. Goldstein, S. Hemming, and R. F. Anderson (2008), Towards explaining the Nd paradox using reversible scavenging in an ocean general circulation model, *Earth Planet. Sci. Lett.*, *274*, 448–461.
Sluijs, A., et al. (2006), Subtropical Arctic Ocean temperatures during the Palaeocene/Eocene thermal maximum, *Nature*, *441*, 610–613.
St. Laurent, L. C., H. L. Simmons, and S. R. Jayne (2002), Estimating tidally-driven mixing in the deep ocean, *Geophys. Res. Lett.*, *29*(23), 2106, doi:10.1029/2002GL015633.
Staudigel, H., P. Doyle, and A. Zindler (1985), Sr and Nd isotope systematics in fish teeth, *Earth Planet. Sci. Lett.*, *76*, 45–56.
Stichel, T., M. Frank, J. Rickli, and B. A. Haley (2012), The hafnium and neodymium isotope composition of seawater in the Atlantic sector of the Southern Ocean, *Earth Planet. Sci. Lett.*, *317–318*, 282–294.
Tachikawa, K., C. Jeandel, and M. Roy-Barman (1999), A new approach to the Nd residence time in the ocean: The role of atmospheric inputs, *Earth Planet. Sci. Lett.*, *170*, 433–446.
Talley, L. D. (1993), Distribution and formation of North Pacific Intermediate Water, *J. Phys. Oceanogr.*, *23*, 517–537.
Taylor, S. R., and S. M. McLennan (1995), The geochemical evolution of the continental crust, *Rev. Geophys.*, *33*, 241–265, doi:10.1029/95RG00262.
Tazoe, H., H. Obata, and T. Gamo (2011), Coupled isotopic systematics of surface cerium and neodymium in the Pacific Ocean, *Geochem. Geophys. Geosyst.*, *12*, Q04004, doi:10.1029/2010GC003342.
Thiede, J., et al. (1981), *Initial Reports of the Deep Sea Drilling Project*, vol. 62, 124 pp., U.S. Government Printing Office, Washington, D. C.
Thomas, D. J. (2004), Evidence for production of North Pacific Deep Waters during the early Cenozoic greenhouse, *Nature*, *430*, 65–68.
Thomas, D. J. (2005), Reconstructing ancient deep-sea circulation patterns using the Nd isotopic composition of fossil fish debris, in *Isotopic and Elemental Tracers of Late Cenozoic Climate Change*, edited by D. Surge and G. Mora, *Geol. Soc. Am. Spec. Publ.*, *395*, 1–12.

Thomas, D. J., and R. K. Via (2007), Neogene evolution of Atlantic thermohaline circulation: Perspective from Walvis Ridge, southeastern Atlantic Ocean, *Paleoceanography*, *22*, PA2212, doi:10.1029/2006PA001297.

Thomas, D. J., T. J. Bralower, and C. E. Jones (2003), Neodymium isotopic reconstruction of late Paleocene-early Eocene thermohaline circulation, *Earth Planet. Sci. Lett.*, *209*, 309–322.

Thomas, D. J., M. Lyle, T. C. Moore Jr., and D. K. Rea (2008), Paleogene deepwater mass composition of the tropical Pacific and implications for thermohaline circulation in a greenhouse world, *Geochem. Geophys. Geosyst.*, *9*, Q02002, doi:10.1029/2007GC001748.

Tomczak, M., and J. S. Godfrey (1994), *Regional Oceanography: An Introduction*, 422 pp., Pergamon Press, London.

Uenzelmann-Neben, G., and K. Gohl (2012), Amundsen Sea sediment drifts: Archives of modifications in oceanographic and climatic conditions, *Mar. Geol.*, *299–302*, 51–62.

van de Flierdt, T., M. Frank, J. R. Hein, B. Hattendorf, D. Gunther, and P. W. Kubik (2004), Deep and bottom water export from the Southern Ocean to the Pacific over the past 38 million years, *Paleoceanography*, *19*, PA1020, doi:10.1029/2003PA000923.

Wareham, C. D., I. L. Millar, and A. P. M. Vaughan (1997), The generation of sodic granite magmas, western Palmer Land, Antarctic Peninsula, *Contrib. Mineral. Petrol.*, *128*, 81–96.

Wijesekera, H. W., and M. C. Gregg (1996), Surface layer response to weak winds, westerly bursts, and rain squalls in the western Pacific warm pool, *J. Geophys. Res.*, *101*, 977–997, doi:10.1029/95JC02553.

Winfrey, E. C., P. S. Doyle, and W. R. Riedel (1987), Preliminary ichthyolith biostratigraphy, southwest Pacific, DSDP Leg 91, in *Initial Reports of the Deep Sea Drilling Project*, vol. 91, edited by H. W. Menard et al., pp. 447–468, U.S. Government Printing Office, Washington, D. C.

Woodard, S., and D. J. Thomas (2009), Is it eolian dust? Contributions to the fine silicate fraction of deep sea sediments on Shatsky Rise, 58Ma, *Geochim. Cosmochim. Acta*, *73*(13), A1452.

Woodard, S., D. J. Thomas, S. Hovan, U. Röhl, and T. Westerhold (2011), Evidence for eccentricity forcing of dust accumulation during the early Cenozoic greenhouse climate interval, *Geochem. Geophys. Geosyst.*, *12*, Q02007, doi:10.1029/2010GC003394.

Wright, J., R. S. Seymour, and H. Shaw (1984), REE and Nd isotopes in conodont apatite: Variations with geological age and depositional environment, in *Conodont Biofacies and Provincialism*, edited by D. L. Clark, *Geol. Soc. Am. Spec. Pap.*, *196*, 325–340.

Wunsch, C., and R. Ferrari (2004), Vertical mixing, energy, and the general circulation of the oceans, *Annu. Rev. Fluid Mech.*, *36*, 281–314.

Zachos, J. C., G. R. Dickens, and R. E. Zeebe (2008), An early Cenozoic perspective on greenhouse warming and carbon-cycle dynamics, *Nature*, *451*, 279–283.

Zeebe, R. E., and J. C. Zachos (2007), Reversed deep-sea carbonate ion basin gradient during Paleocene-Eocene thermal maximum, *Paleoceanography*, *22*, PA3201, doi:10.1029/2006PA001395.

Zhou, L., and F. T. Kyte (1992), Sedimentation history of the South Pacific pelagic clay province over the last 85 million years inferred from the geochemistry of Deep Sea Drilling Project Hole 596, *Paleoceanography*, *7*, 441–465, doi:10.1029/92PA01063.